第 49 卷第 2 期
七月 2024

Vol. 49 No. 2
Oct - Dec 2024

Diqiu Kexue - Zhongguo Dizhi Daxue Xuebao/Earth Science
Journal of China University of Geosciences
https://dqkx-periodicals.com

DOI: 10.5281/zenodo.14543618

Evaluation of Landsat 9 and Sentinel 2 Spectral Reflectance Calibration Validation over Tropical Region

Andie Setiyoko[a], Hendayani[a], Heri Sulyantara[a], Ahmad Maryanto[b], Dianovita[a], Musyarofah[b], Bayulodie Vallianto[c], Kiki Winda Veronica[a], Ahmad Luthfi Hadiyanto[a], Suhermanto[b], Erna Sri Adiningsih[b], Andy Indradjad[b], Dinari Nikken Sulastrie Sirin[b], A. Hadi Syafrudin[b], Patria Rachman Hakim[b], Wahyudi Hasbi[b]

[a]National Research and Innovation Agency (BRIN), OREI, Research Center for Geoinformatics, Jl. Raya Bogor km 46, Cibinong, Indonesia, 16911
[b]National Research and Innovation Agency (BRIN), ORPA, Research Center for Satellite Technology, Jalan Cagak Satelit No.8 km 0, Bogor, Indonesia, 16310
[c]National Research and Innovation Agency (BRIN), DIRI, Directorate of Laboratory Management, Research Facilities and Science and Technology Areas, Jl. Raya Bogor km 46, Cibinong, Indonesia, 16911

Corresponding author at: andie.setiyoko@brin.go.id

Received: 30 October 2024
Accepted: 28 November 2024
Published: 23 December 2024

Abstract: Satellite image calibration and validation over tropical areas are rarely considered in the research area. Most of the processes are in the non-tropical area. In this research, we would like to perform mixed calibration and validation methods; both cross and vicarious validation are mixed to understand the case better. The data used are Sentinel-2 and Landsat-9, categorized as middle-resolution imagery. Since the data are available to the public, both are familiar and widely used by the researcher and user. Therefore, it is required to gain the radiometric validation of those data. It is proposed that a mixed method of cross and vicarious calibration and validation of the satellite imagery be introduced. To gain experience in the process, specific objects are chosen based on several conditions that fulfill previously studied criteria. After conducting the analysis based on each spectral BOA reflectance of the data, both observed and predicted reflectance values statistically have no significant differences after the processing applied. Landsat 9 and Sentinel 2 reflectance values are relatively similar according to the process result. However, the BOA reflectance values measured showed different values in small wavelength ranges. The T-test of three pairs in the mixed method shows no statistically significant difference between predicted and observed spectral reflectance.

Keywords: *Spectral reflectance, tropical area, calibration, validation*

1. Introduction

The remote sensing data processing mechanism is carried out through several stages before it becomes information that users can use directly. After the satellite image is acquired, initial processing (pre-processing) is carried out which consists of radiometric correction and geometric correction. Radiometric correction is carried out to produce reflectance values with minimal error, whether errors are caused by atmospheric influences, clouds and their shadows, terrain, and so on. Meanwhile, geometric correction is conducted to produce georeferenced images with an accuracy level according to the processing method used. This research tests the quality of reflectance values produced by the existing processing processes at the National Research and Innovation Agency (BRIN).

In line with this, a study is needed regarding the calibration tests of satellite images that have been acquired by the National Aeronautics and Space Institute (LAPAN) previously and BRIN currently (Inggit Lolita Sari, Tatik Kartika, 2011; Sari et al., 2022). Calibration tests are needed to provide information on the quality of a satellite image in the form of geometric and radiometric accuracy. For example, the USGS periodically carried out Landsat calibration tests and other images (Falls, 2010; Helder et al., 2012) in designated areas. Regarding calibration and validation tests in Indonesia, this is still not optimal. The character of the tropical Indonesian region, which has a unique biodiversity and the phenomenon of particular natural resource content, is considered reflective. That's why this research needs to be done. A reflectance value calibration test is required for all types of satellite imagery to determine the extent to which the reflectance value of the image resulting from initial processing so far has represented the actual condition of the object in the field (Sari et al., 2022).

Concentration calibration tests will be performed on medium-resolution images as a first step. In 2022, the research team conducted calibration tests in the area. However, weather factors still have an influence. Clear weather is essential when calibrating satellite images. In 2023, it was planned to carry out image calibration in the hot or dry season when the satellite makes acquisitions in this area. In 2024, calibration tests will be carried out on other images to increase confidence levels in using pre-processed satellite images.

The calibration results will be used as validation material for the image to determine the difference in reflectance values and actual conditions in the field. Literature studies were conducted systematically before the calibration process so that the results obtained comply with the standards based on the previous research.

Earth observation monitoring using middle-resolution satellite imagery is considered the most efficient breakthrough in the past forty decades (Markham et al., 2012). This experience is proven for most countries, particularly for unreachable areas such as mountains or forests, which are almost tropical. The demand for middle-resolution satellites is widespread in various sectors of the application. The highest request is from the environmental monitoring department, followed by the forestry monitoring institution, the agriculture sector, and more. For instance, monitoring the carbon stock account requires these imageries for large regions annually. An updated example is INCAS (Indonesia National Carbon Accounting System), which processes optical satellite images (Inggit Lolita Sari, Tatik Kartika, 2011; Sari et al., 2022) to develop multiyear carbon stock monitoring for such tropical countries' forests and the Indonesian region, for instance (Inggit Lolita Sari, Tatik Kartika, 2011; Sari et al., 2022). The paddy field harvest monitoring systems are also developed using middle-resolution satellite imagery (Area et al., 2023). Therefore, continuous programs ensuring this image availability worldwide are required.

There are some advantages of using middle-resolution data: first is the wider area covered due to the long swath width; second, is the spectral quality of the sensor divided into multispectral bands; and third, almost all this type of data is accessible to the public user. There are several middle-resolution satellites, e.g., Landsat generation, SPOT satellites, IRS satellites, ALOS optical series, and others. The most known pioneer in the field is Landsat satellites. Landsat has been operated since 1972 (Teixeira Pinto et al., 2019) from its first generation until when Landsat 9 was launched on September 27, 2021. This latest generation produces data similar to Landsat 8. Both satellites carry Operational Land Imager (OLI) sensors containing 9 multispectral bands, which are the subjects of analysis in this experiment (Tang et al., 2019).

According to the widely used Landsat 8/9 imagery, it is urgently required to conduct the calibration and validation processes to gather sufficient information on the accuracy of spectral reflectance produced from the existing image acquisition and processing system. Several experiments have been conducted in several areas (Chander et al., 2004; Liu et al., 2017; Martimort et al., 2012; Salaswati et al., 2021; Teixeira Pinto et al., 2019). The overall result shows that the Landsat 8 spectral reflectance is 5 % accurate (Liu et al., 2017). The experiment also shows that calibration and validation of Landsat 8/9 in the tropical area are crucial to be conducted. Therefore, this research aims to fill the gap by further analyzing the calibration and validation process.

Several calibration and validation techniques have been applied in previous research. The initial method proposed was PICS (pseudo-invariant calibration sites) absolute calibration model (Helder et al., 2012). Then, cross-calibration/validation analysis was conducted for Landsat 8 imagery (Liu et al., 2017). Later, radiometric cross-calibration was experimented for Landsat-8 OLI (Area et al., 2023). Multiple Pseudo Invariant Calibration Sites (PICS) were applied to simulate observations of Landsat 8 using Earth Observing-1 (EO-1) Hyperion hyperspectral reflectance (Raut et al., 2019). All methods study areas are mostly located in non-tropical areas.

Several methods for the calibration and validation processes mainly focus on four main types of measurement: onboard (Song et al., 2022), cross (Lu et al., 2022), vicarious (Concha et al., 2019; Liu et al., 2017), and Rayleigh (Zhu et al., 2022). Each technique has been applied to calibrate various kinds of satellite imagery. In this research, we would propose mixed cross and vicarious calibration. The experiment we propose attempts to perform calibration and validation involving multiple satellite images acquired over a single tropical region. The data involved processed bottom-of-atmosphere (BOA) images of Landsat 9 and Sentinel 2, which involved land observation measurement and a multi-analysis using the existing method mixed with additional T-Test analysis. T-test analysis is statistical processing to compare two distribution data for similar sources (Zhang et al., 2021). The additional analysis is addressed to enrich the existing calibration and validation method.

The structure of the paper is divided into five sections. The first is the introduction section, which explains the scientific background and the research objectives. The second section describes the research method, the specification of data used, and the tools used for land measurement. This section is followed by the result and analysis section, which shows the results of both land observation and image processing and the brief analysis described. The most important part of the paper is in the discussion section, where the discussion related to the result of the experiment is expressed and connected with the most recent findings related to the calibration and validation process. The last section is the conclusion, which summarizes all sections and marks out further challenging research.

2. Methodology

The methodology was developed based on 4 main stages: satellite image selection, field measurement, image processing, and comparison analysis.

2.1 Satellite Image Selection

In this research, we plot the study area in the tropical zone, which fulfilled the term conditions applied based on previous research (Ong et al., 2018)(Salaswati et al., 2021).

This research involves 2 medium satellite images: Landsat 9 and Sentinel 2. We validate Landsat 9 and Sentinel 2 using field measurement to develop a novel mixed method of calibration and validation method. Landsat 9 satellite has OLI-2 design, a copy of Landsat 8's OLI. Landsat 9 supplies imagery persistent with preceding Landsat's spectral, spatial, radiometric, and geometric qualities. OLI-2 contributes data for nine spectral bands with a maximum ground sampling distance (GSD), both in-track and cross-track, of 30 meters (m) (98 feet) for all bands except the panchromatic band, which has a 15-meter (49 feet) GSD. To assure the accuracy and stability of radiometric quality, OLI-2 is equipped with internal calibration sources and the capability to carry out solar and lunar calibrations as well.

The specification of Landsat 9 spectral is shown in Table 1 (USGS, 2022).

Table 1 *Landsat 9 Spectral Specification*

Band	Detail	Wavelength
1	Visible Coastal Aerosol	(0.43 - 0.45 µm) 30-m
2	Visible Blue	(0.45 - 0.51 µm) 30-m
3	Visible Green	(0.53 - 0.59 µm) 30-m
4	Red	(0.64 - 0.67 µm) 30-m
5	Near-Infrared	(0.85 - 0.88 µm) 30-m
6	SWIR 1	(1.57 - 1.65 µm) 30-m
7	SWIR 2	(2.11 - 2.29 µm) 30-m
8	Panchromatic (PAN)	(0.50 - 0.68 µm) 15-m
9	Cirrus	(1.36 - 1.38 µm) 30-m

The Landsat 9 imagery continuously focuses on acquiring data managed for worldwide observations, including monitoring, understanding, and managing Earth's natural resources (USGS, 2022). Landsat 9 has a significant advantage in spectral

imagery; the images have sharper visualization than other satellite imagery. Landsat has proven a spectral reference for various middle-resolution satellites. Most of the satellites only consist of 4 bands: red band, green band, blue band, and near-infrared band; however, Landsat generation has more than 4 bands. This research involves Landsat 9 multispectral imagery consisting of band 1, band 2, band 3, band 4, band 5, band 6, and band 7.

The next popular middle-resolution satellite image data developed by ESA that is feasible for the public is Sentinel 2. This satellite is aimed at monitoring Earth's resources. It has a spatial resolution of 10 m, better than Landsat 9.

The spatial resolving power of the Sentinel-2 Mission and its payload MSI instrument are divided into three main groups of categories: 10 m, 20 m, and 60 m. The temporal resolution of a satellite in its trajectory is the frequent repetitiveness of the spacecraft to an appropriate spot. Each single Sentinel-2 satellite has a revisit frequency of 10 days, and a combined constellation satellite has a revisit frequency of 5 days.

Every imaging sensor has a spatial resolution, defined as the at-ground representation of an individual object detected in a satellite sensor array. The higher the spatial resolution of an instrument, the better its ability to distinguish objects. The spectral resolution illustrates the instrument's ability to differentiate spectra elements in the electromagnetic spectrum. The radiometric resolution of an imaging device is a measurement of the accumulative level of intensity or reflectance that can be exhibited or discriminated by the system. The higher the radiometric resolution, the greater the device's capability to identify dissimilarity in intensity or reflectance. Sentinel-2 has a swath width of 290 km. In contrast, Landsat 5 TM and Landsat 7 ETM+ have a swath width of 185 km, and SPOT-5's swath width is 120 km. Table 2 (ESA, 1956), (Martimort et al., 2012) shows its specifications and details.

Both images are covered in the study area of Bromo sand on the same date of acquisition, 14 June 2023. The image covered the area in the summer season, which was assumed free of clouds. It was acquired on 14 June 2023 and covered the Bromo area. The scene ID number of the Landsat 9 satellite image is LC09_L1TP_118065_20230614_20230614_02_T1. The path/row of the image is 118/065. The Sentinel 2A satellite image ID number is S2_T49MGM_118065_20230614. Both images are shown in Figure 2.1. This research involves Sentinel 2 multispectral imagery consisting of band 1, band 2, band 3, band 4, band 5, band 6, band 7, band 8A, band 11, and band 12.

Table 2 *Sentinel 2 Spectral Specification*

Spatial Resolution	Detail	Wavelength
4 x 10 m Bands	The three classic visible RGB bands	(Blue (~493nm), Green (560nm), and Red (~665nm)) and a Near Infra-Red (~833nm) band
6 x 20 m Bands	To monitor snow/ice/cloud detection or vegetation moisture stress assessment	4 narrow Bands in the VNIR vegetation red edge spectral domain (~704nm,~740nm, ~783nm, and ~865nm) and 2 wider SWIR bands (~1610nm and ~2190nm)
3 x 60 m Bands	Focused for cloud screening and atmospheric correction	(~443nm for aerosols and ~945nm for water vapour) and cirrus detection (~1374nm)

Both images are relatively clear of cloud and haze, especially in the study area, Bromo Mountain. This site was chosen due to the homogeneous objects in the area. The object is mountain sand of around 150m x 150m, which is planned to be fit for spectrometer land measurement.

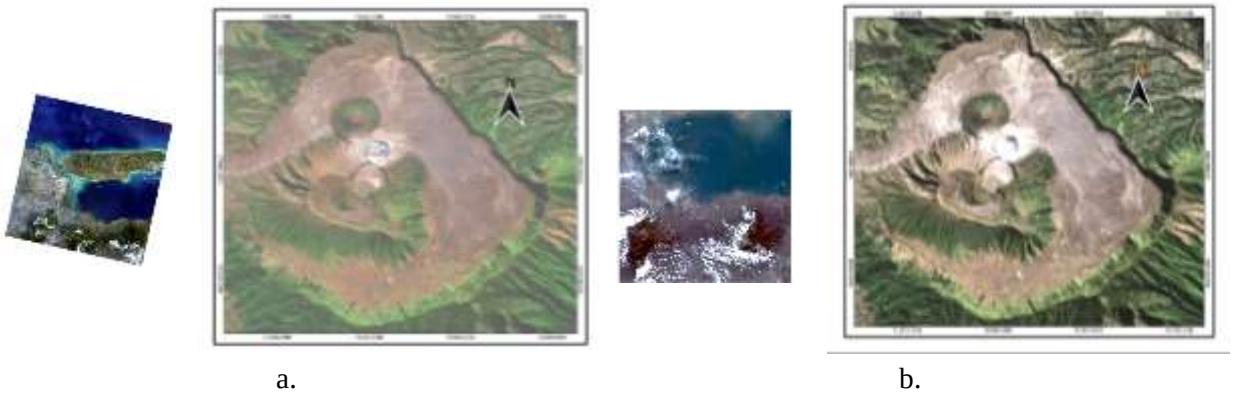

a. b.

Figure. 2.1 *a. Landsat 9 images of the study area and b. Sentinel 2 images of the study area.*

2.2 Field Measurement

The main tool in the measurement process is a spectroradiometer. In this research, we choose ASD field spec shown in Figure 2.2. The 3 nm VNIR, 8 nm SWIR spectral resolution of the ASD FieldSpec. 4 Hi-Res spectroradiometer gives preferable spectral performance over the entire solar irradiance spectrum (350 – 2500 nm). The upgraded spectral resolution in the SWIR range (1000 – 2500 nm) is applicable for recognizing and identifying compounds with narrow spectral features in longer wavelengths, such as the transformation of mineralogy and gases for atmospheric analysis (Malvern Panalytical, 2022). The tool for measurement belongs to BRIN. Other tools are GPS handheld receivers, digital cameras, and others.

Figure. 2.2 *ASD FieldSpec 4 Hi-Res spectroradiometer (https://www.malvernpanalytical.com/)*

The observation scenario is based on the standard measurement method (Liu et al., 2017; Ong et al., 2018). The result of the observation is spectral radiance and reflectance of the object directly generated from the measurement tool and processed by ViewSpecPro software.

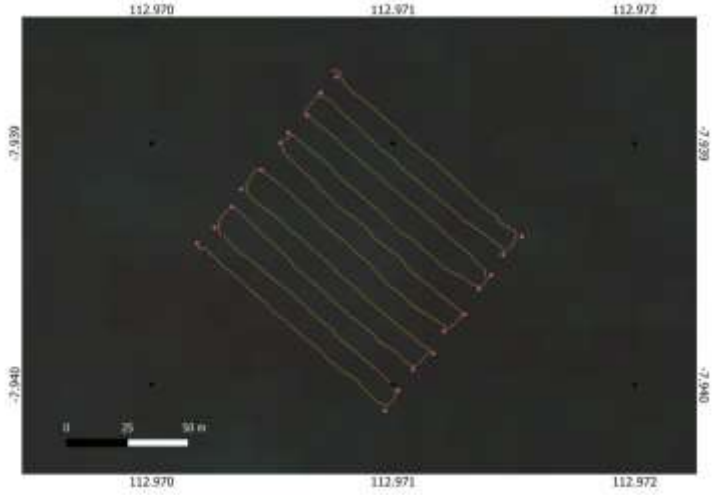

Figure. 2.3 *Field measurement tracking*

Figure 2.3 is the tracking of the measurement to gain the spectroradiometer value. Several procedures have been fulfilled (Ong et al., 2018):

- The measurement location, by preference, should own limited vegetation or be completely without vegetation. Another preferable site should include homogenous plant life, such as grassland. Crops should be prevented.
- The site should contain a homogeneous object with an area of 100 x 100 m (3 x 3 pixels area, 1 ha). The area comprises brightness levels and low-height surface covers with minimum topography.
- The place should be located at least 100 m from roads, power lines, or other factors.
- The spots should be conveniently approachable.
- The aerosol effects must be regarded. The consideration of aerosol impacts should not be used to restrict measurements.
- Cloud cover and frequency of cloud cover should be considered.

The procedures have been examined to plan land observation measurements. The location is in the Bromo sand area, which has a homogenous land cover for a large area. The land observation was conducted at 09.50 Western Indonesian Time (local time), 10 minutes before the satellites passed over the area for the acquisition process. The land observation process takes about 30 minutes. The operators carried the spectroradiometer and navigation tools along the dedicated path, as shown in Figure 2.4.

Figure. 2.4 *Land observation*

2.3 Experiment

The experiment is based on the flowchart shown in Figure 2.5. Previous literature is the basis of the developed flowchart. The methodology used three data sources: Landsat 9, Sentinel 2, and reflectance derived from land observation. Landsat 9 data consists of the Operational Land Imager (OLI) bands and spectral reflectance and radiance measured in the field observation. Spectral reflectance was derived from Landsat 9 imagery as the predicted values, and the measured reflectance was the observation data, along with Sentinel 2.

The flowchart developed from previous research experiments has been conducted only using 1 type of satellite image data (Setiyoko et al., 2023).

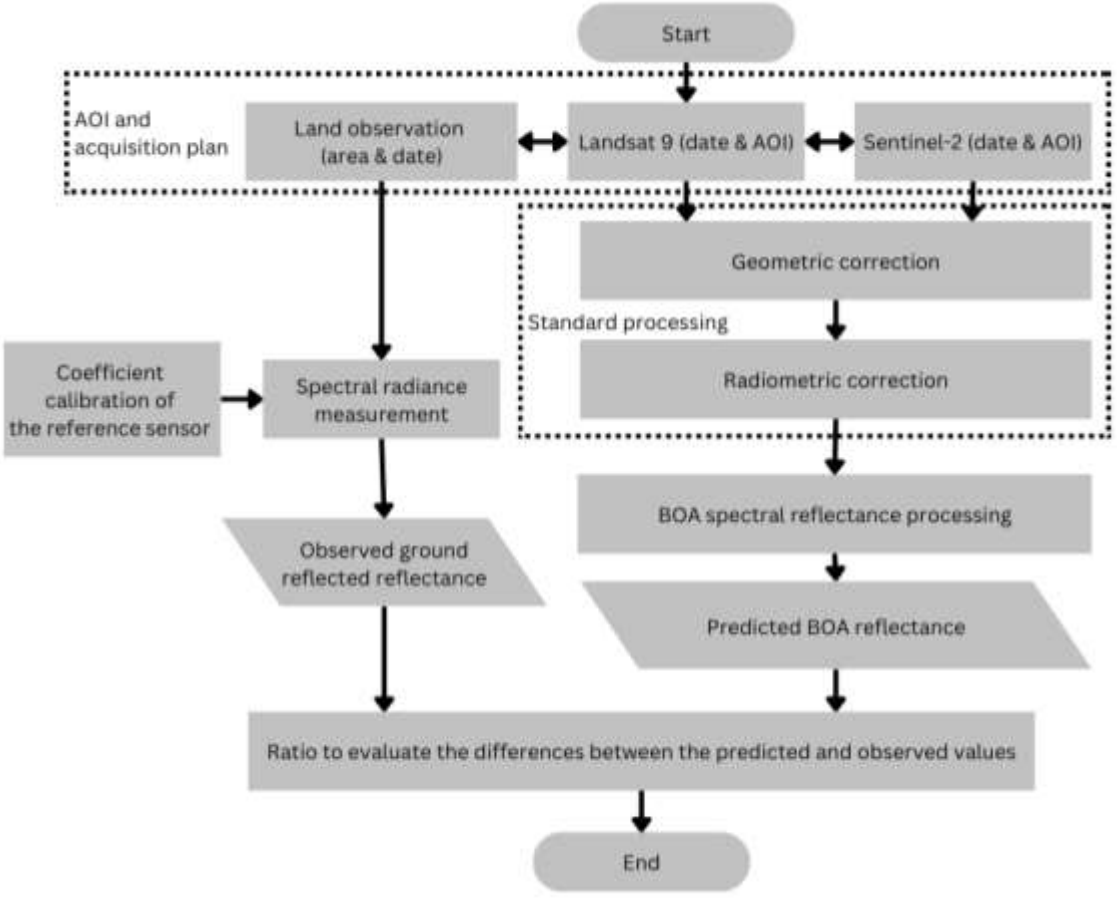

Figure. 2.5 *Middle-resolution calibration and validation process*

The methodology process consists of 4 main stages:

- Determining the area of measurement based on a homogeneous object in about 150m x 150m. The area assumed could cover 5x5 pixels of Landsat multispectral image.
- Determining the date of land measurement based on a satellite sensor was programmed to acquire the image in the area selected from No.1. and the cloud-free prediction based on the weather forecast.
- Land observation in the study area using the spectroradiometer and the supporting equipment. The output is the spectral radiance of the field object.
- Standard image processing starts with geometric correction, then radiometric correction and the last is spectral radiance and reflectance image processing. The output is spectral radiance and reflectance of the images.
- The last stage is a comparative analysis of the two values derived from the field and image processing to gain the coefficient value and correct the spectral value of the imagery processed in the system.\

2.4 Image Processing

To generate predicted spectral radiance and reflectance from Landsat 9 image, TOA radiance and reflectance calculation were processed based on the USGS documentary (USGS, 2022). Landsat 9 Level-1 data were transformed to TOA spectral radiance by utilizing the radiance adjustment factors in the MTL file. The transformation employs the following equation (USGS, 2022). The formula of conversion to TOA Radiance is as follows (USGS, 2022).

$$L_\lambda = M_L Q_{cal} + A_L \quad (1)$$

Where L_λ is TOA spectral radiance (Watts/ (m2 * srad * μm)), M_L is band-specific multiplicative adjustment factor from the metadata, A_L is a band-specific additive rescaling factor from the metadata, Q_{cal} is quantized and calibrated standard product pixel values (DN).

The formula of conversion to TOA Reflectance is as follows (USGS, 2022).

$$\rho\lambda' = M_L Q_{cal} + A_\rho \quad (2)$$

Where, $\rho\lambda'$ is TOA planetary reflectance, without correction for solar angle, M_L is *a* band-specific multiplicative rescaling factor from the metadata, A_ρ is Band-specific additive rescaling factor from the metadata, Q_{cal} is quantized and calibrated standard product pixel values (DN).

TOA reflectance with a correction for the sun angle is then:

$$\rho\lambda = \frac{\rho\lambda'}{\cos(\theta_{sz})} = \frac{\rho\lambda'}{\sin(\theta_{sE})} \quad (3)$$

Where $\rho\lambda$ is TOA planetary reflectance, θ_{sE} is Local sun elevation angle, and θ_{sz} is Local solar zenith angle.

Image processing tools are QGIS software, and the result of the processing experiment is a predicted reflectance value based on the Landsat 9 OLI bands.

The reflectance converter for Sentinel 2 is based on the formula in the SNAP software developed specifically for image processing. The formula is as follows (ESA, 1956).

$$R_{TOA}(\lambda) = \frac{\pi L_{TOA}(\lambda)}{E_0(\lambda)\cos(\theta)} \quad (4)$$

Where E_0 and θ are the solar spectral irradiance and the sun's zenith angle, respectively. The conversion from reflectances to radiances follows the inverse of this equation.

The formula to derive the representative value of the reflectance for each band for comparison analysis is as follows.

$$\bar{r} = \frac{1}{b-a}\int_a^b r\, dw \quad (5)$$

Where, $a - b$ is the range of wavelength, r is the reflectance value of wavelength w to get the average reflectance value, $\bar{r}$.

Landsat 9 and Sentinel 2 reflectance images have been atmospheric correction processed into BOA reflectance images which can then be verified with field measurement results. Previously, both images were also geometrically corrected systematically.

2.5 Comparison Analysis

Scenario to compare the validation process of the predicted spectral reflectance value, the statistical-based comparison method, and T-test analysis are exercised in the experiment as the statistical cross-analysis. Several scenarios for validation are using ratio analysis and T-test analysis. The ratio analysis formula is as follows (Liu et al., 2017).

$$\text{Comparison Ratio} = \frac{Predicted\ Value}{Observed\ Value} \quad (6)$$

Then, the method for comparing two sample means is the t statistic and the degrees of freedom for choosing the tabulated t-value. The formula is given by (Ellis, 2014).

$$t = \frac{\bar{x}_1 - \bar{x}_2}{\sqrt{\frac{{s_1}^2}{n_1} + \frac{{s_2}^2}{n_2}}} \quad (7)$$

In this case, we require two separate sample means $\bar{x}$, standard deviations s, and sample sizes n. The number of degrees of freedom (DOF) is computed using the formula (Akhilesh Ganti, 2022).

$$dof = n - p \quad (8)$$

p is the number of different parameters or relationships. As for the notation, the prediction value would be annotated as 1 and the observation value as 2. The processing was performed using Microsoft Excel software.

As for the result of the T-test, there are two options available; there is no statistically meaningful dissimilarity between the two samples if the value of the T-test is lower than the critical value in the T-table (Junaidi, 2010), and there is no if the previous condition is not fulfilled in the hypothetical assumption.

3. Result and Analysis

Based on the methodology developed, several outputs are produced to be analyzed. The Landsat 9 image processing system outcomes its reflectance image using the formulas 3 and 4. The Sentinel 2 BOA reflectance image is also generated using the SNAP software. Then, the object's radiance and reflectance data were collected for the mixed calibration and validation process. To concentrate on the land measurement object, the pixels on both images were selected to be analyzed.

Several pixels located on the spectrometer measurement field were selected to be analyzed. Eighteen pixels of Landsat 9 multispectral images (7 bands in the same spatial resolution) were processed using the formula of TOA reflectance. Several Sentinel 2 multispectral data pixels were selected also.

Based on the land observation measured, the radiance and reflectance of the object are collected. It is processed using ViewSpecPro software. The radiance of the object measured has a precision of 1 nm or 0.001 µm. The result is shown in Figure 3.3.

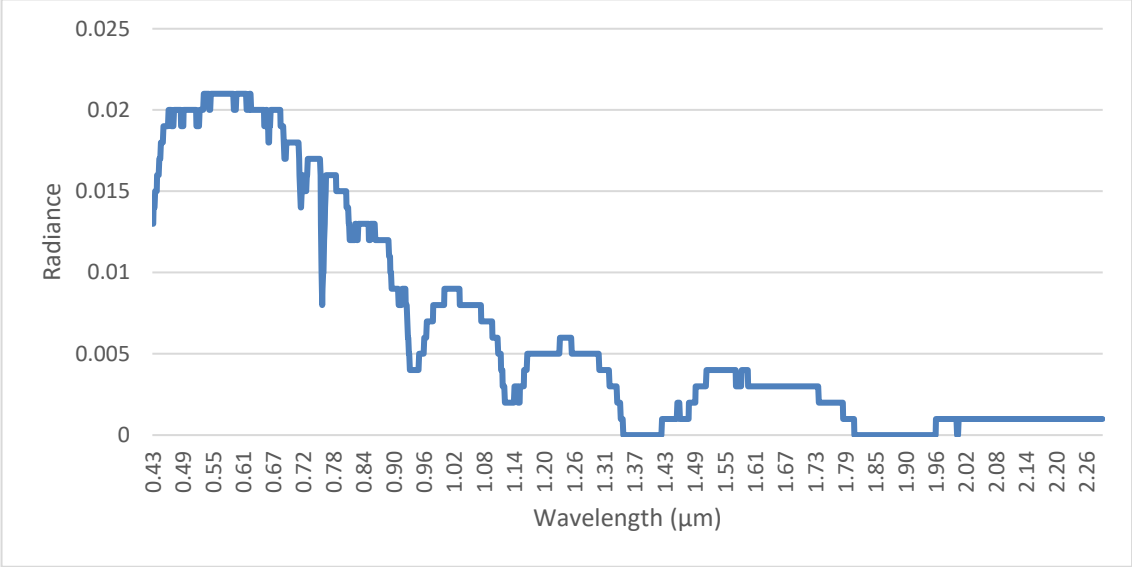

Figure. 3.3 *The radiance of the object generated from land observation*

The object is sand located in the plain area of a tropical mountain area. Reflectance is generated, also shown in Figure 3.4.

3.1 Spectral Reflectances of Landsat 9, Sentinel 2, and field observation

Several results were generated from the experiment. The first is spectral reflectance generated from object observation using the ASD field spec shown in Figure 3.4. The figure that the reflectance of an object is selected from wavelength 0.43 µm to 2.20 µm. The value of the reflectance starts from 0 to around 0.16. The value distribution looks smooth at the lower wavelength and slightly increases and decreases between 0.43 and 1.26 µm. After reaching wavelength value 1.37 until 2.0 µm, the reflectance value fluctuates. Several wavelength ranges have 0 reflectance values and extreme reflectance values. The phenomenon might detected as spectral noises due to the atmospheric window effect (Pal & Porwal, 2015). As we can see in the spectral radiance (W/m2/sr/nm) of the object shown in Figure 3.3, there are some 0 values in several wavelength ranges.

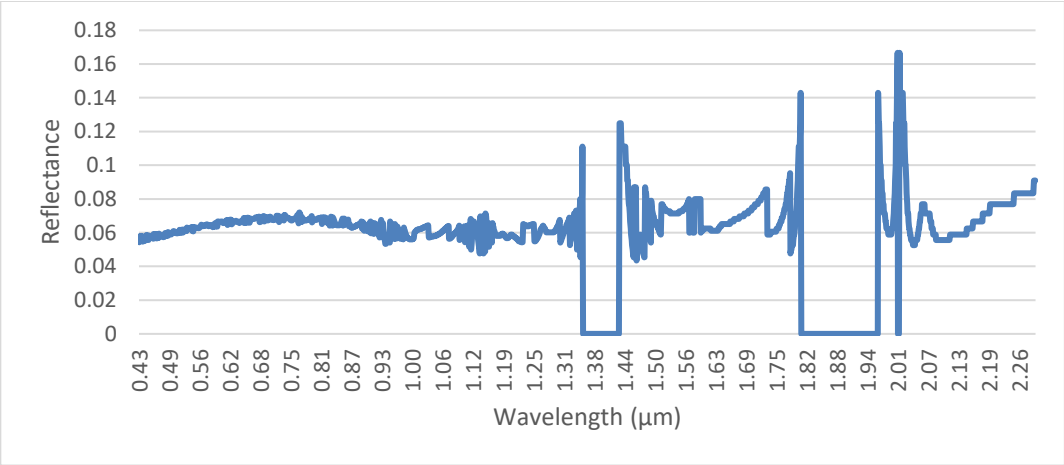

Figure. 3.4 *The reflectance of the object object generated from land observation*.

The second results from the processing are Landsat 9 TOA and BOA reflectance generated from the original/raw data using formulas 2 and 3. Based on the selected pixels on the land observation area, the averaged reflectance values of Landsat 9 are derived from selected pixels, as shown in Figure 3.5 for band 1, band 2, band 3, band 4, band 5, band 6, and band 7.

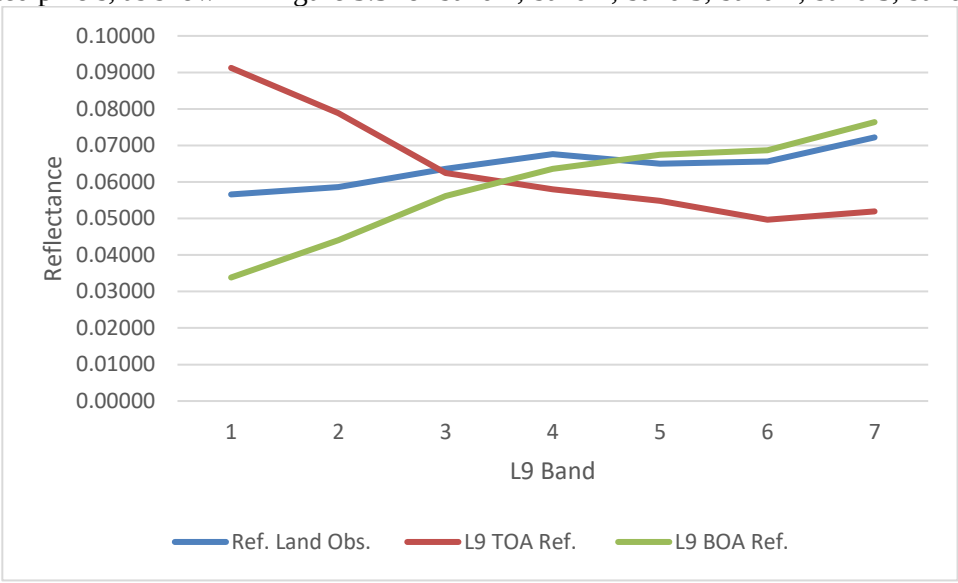

Figure. 3.5 *Landsat 9 BOA reflectance value*

Meanwhile, the averaged TOA and BOA reflectance values of Sentinel 2 of the study area are also generated for all available bands, as shown in Figure 3.6.

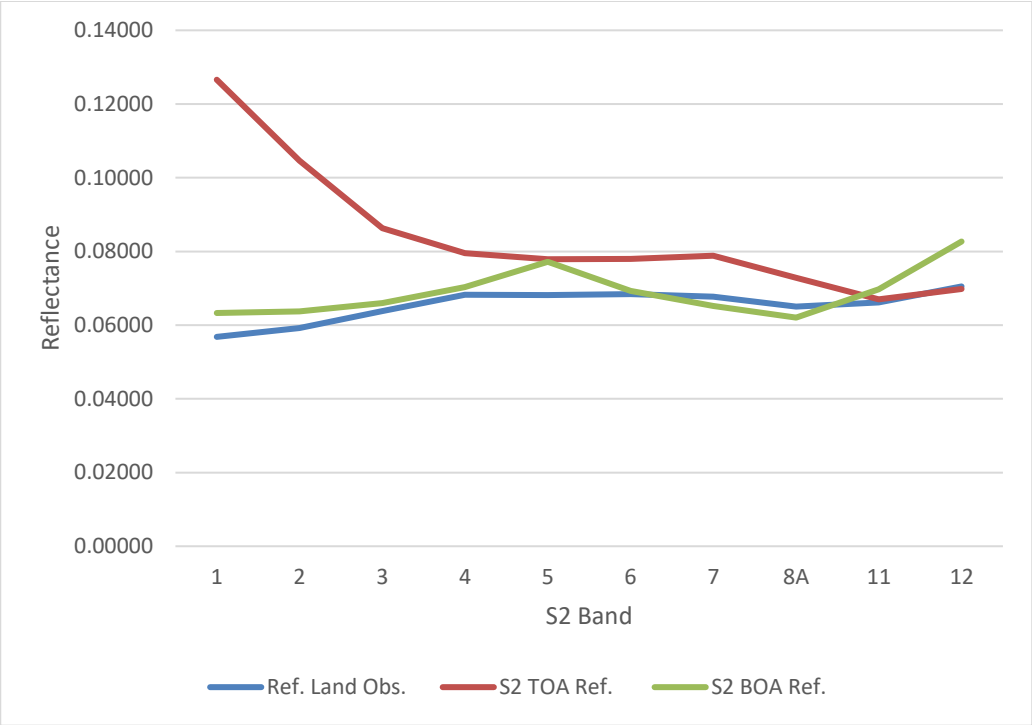

Figure. 3.6 *Sentinel 2 BOA reflectance value.*

The mixed cross and vicarious calibration and validation comparison is developed based on the spectral band of each satellite image. The representation value of spectral reflectance from land observation is generated using averaging or an integral approach, formula 8. The value is compared with the spectral reflectance generated from the satellite image calculated using the same formula. According to Figure 3.5 and Figure 3.6, BOA reflectances of Landsat 9 and Sentinel 2 are more identical to land observation reflectance.

3.2 Comparison of Landsat 9, Sentinel 2, and field observation reflectance

The averaged values of reflectance derived from the images and land measurements are shown in Figure 3.7. According to the figure, the reflectance values of Landsat 9 and Sentinel 2 have similar numbers for almost all wavelength ranges, while the observed reflectance has different numbers on smaller wavelengths. However, the reflectance values on the middle and bigger wavelengths are slightly similar.

Based on formula 5, the ratio between the reflectance data is presented in Table 4. The result is analogous to the previous analysis that Sentinel 2 and Landsat 9 have similar values. The results of the T-test analysis between pairs of reflectance data are in Table 5.

Almost all pairs' t-test values are less than the t-table value; therefore, there is no statistically significant difference between predicted and observed spectral reflectance.

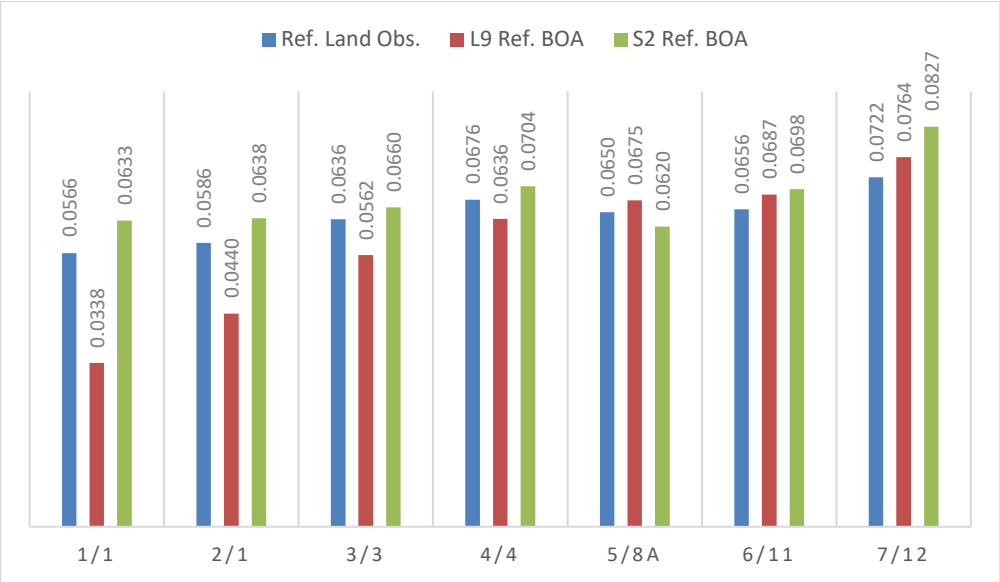

Figure. 3.7 *BOA reflectance value of the data*

Table 3 *The ratio value between the data*

Band Landsat 9/ Sentinel 2	Ratio S2/Obs.	Ratio L9/Obs.	Ratio S2/L9
1/1	1.1182	0.5980	1.8700
2/1	1.0875	0.7512	1.4476
3/3	1.0389	0.8837	1.1756
4/4	1.0408	0.9407	1.1064
5/8A	0.9543	1.0376	0.9197
6/11	1.0632	1.0469	1.0156
7/12	1.1452	1.0580	1.0825

Table 4 *T-Test value between the reflectance data*

Pair	T-test value	T-table value
Land Obs-S2	0.3724	2.22814
Land Obs-L9	0.2445	2.22814
S2-L9	0.1493	2.22814

The reflectance value relatively decreases slightly from band 1 up to band 7. The higher the wavelength, the lower the reflectance value. This condition is similar to the reflectance signature of the desert sand of previous research in some particular time observation (Liu et al., 2017). Based on both results, the cross-statistical analysis is conducted using T-test analysis. The ratio is high in band 1 and decreases slightly up to band 7. The best ratio is near 1, which is in band 3. Then, the ratio decreases until band 7.

The value in Table 4 shows the ratio between the predicted value and the observed value. Ratio 1 means there are no differences between the two values. The ratio of band 3, 1.0389, is nearly close to 1. It is also for band 4 and band 5. This is assumed due to the sensitivity of band 3 for sand as an object of measurement.

Furthermore, the T-test analysis was calculated for Landsat 9 and land observation based on formula 6; the result was 0.2445, and the T-table was 2.22814, with a probability value of 0.025 and a degree of freedom of 10 (Junaidi, 2010), due to < means there is no statistically significant difference between predicted spectral reflectance and observed spectral reflectance. Therefore, the predicted spectral reflectance of the processed Landsat 9 image statistically does not significantly differ from the measured spectral reflectance based on this experiment.

The reflectance value of Sentinel 2 and observation have a significant gap on the smaller wavelength. It becomes close, starting at band 3 to 8A, and then at band 9, both values have a gap again. However, band 11 and 12 values are similar.

Based on formula 5, the ratio between the reflectance data generated from Sentinel 2 and land observation is presented in

Table 6. Based on the ratio analysis shown in the table, almost all band ratio values are near to 1 except for band 1, band 2, and band 9.

Therefore, the reflectance values of Sentinel 2 are approximately fit to the land observation reflectance. Furthermore, the T-test analysis between the complete band of Sentinel 2 and the land observation reflectance is 0.3724, and the T-table is 2.17881. Therefore, there is no statistically significant difference between predicted and observed spectral reflectance.

4. Discussion

Based on the analysis result almost all bands, whether in Sentinel 2 or Landsat 9, are relatively identical in reflectance values, except for lower bands: band 1 and band 2 for near-equatorial tropical areas, in this case in the sand area, at the top of the mountain of Bromo, East Java, Indonesia. This finding is similar to previous research in high-latitude regions (Chen & Zhu, 2022), for the middle latitude, China (Cao et al., 2022), and also in the European region (Trevisiol et al., 2024).

The proposed method, mixed cross-vicarious calibration and validation for middle-resolution satellite imagery in this case the last generation of Landsat and Sentinel 2 using land observation reflectance data brings more valuable information. Based on three sources of reflectance data, an analysis has been conducted, visible bands derived from both data, Landsat 9 and Sentinel 2 have similar reflectance values with land observation reflectance. This could be an advantage compared to previous methods to support harmonization between satellite imageries, particularly for middle-resolution images (Cao et al., 2022).

5. Conclusion

According to the statistical cross-analysis, it could be concluded that the spectral reflectance derived from Landsat 9 OLI bands and Sentinel 2 are relatively valid. The value between the predicted and the observed values has no significant differences. There might be noises from the field due to atmospheric conditions that affect the field measurement tools, particularly in lower wavelengths. Further analysis would be improved in future research. Several comparisons using other types of similar satellite images would be applied, for instance, Sentinel 2 at the same area of interest. Several additional objects would be added for calibration and validation, and, importantly, unique signature reflectance that could only be found in the tropical region.

Further research might be interesting in calibration and validation for more types of land objects, including biodiversity in the tropical region; otherwise, calibration and validation for other classes of remote sensing spatial resolution.

Overall, the findings of this research could be essential for various fields of remote sensing technology divisions for both scientists and practitioners. The result could provide important information as feedback for satellite providers of Landsat 9 and Sentinel 2 in evaluating their products, particularly for tropical region data acquisition. Furthermore, it would support their planning and development program for the next generation of middle-resolution satellites. Internally, the result could be based on research for developing our constellation satellite. In the application field, the result information is also feedback for our image processing facilities which operate to process data from raw images acquired by the ground station to the analysis-ready data (ARD) served for public use. These data contribute to multiple applications such as agriculture, environmental monitoring, urban planning, and disaster mitigation. Research on satellite image calibration and validation brings challenges for the various topics of research activities. In the tropical region, we could provide calibration validation infrastructures for satellite providers. Several places could be the sites for the operation. Other than that, there is also the opportunity to calibrate and validate high-resolution satellite images as well as synthetic aperture radar (SAR) images in the region.

Acknowledgments

Appreciation for Pusdatin-BRIN and USGS for the satellite imagery data, DIRI-BRIN for the spectroradiometer tool, and BBTNBTS for the land observation permission.

6. References

Akhilesh Ganti, S. K. (2022). Degrees of Freedom in Statistics Explained: Formula and Example. *Degrees of Freedom in Statistics Explained: Formula and Example*. https://www.investopedia.com/terms/d/degrees-of-freedom.asp

Area, P. F., Muchsin, F., Pradono, K. A., Prasasti, I., Ulfa, K., & Winda, K. (2023). *Effect of Atmospheric Correction Algorithm on Landsat-8 and Sentinel-2 Classification Accuracy in Paddy Field Area*. *20*(1), 58–66.

Cao, H., Han, L., & Li, L. (2022). Harmonizing surface reflectance between Landsat-7 ETM + , Landsat-8 OLI, and Sentinel-2 MSI over China. *Environmental Science and Pollution Research*, *29*(47), 70882–70898. https://doi.org/10.1007/s11356-022-20771-4

Chander, G., Helder, D. L., Markham, B. L., Dewald, J. D., Kaita, E., Thome, K. J., Micijevic, E., & Ruggles, T. A. (2004). Landsat-5 TM reflective-band absolute radiometric calibration. *IEEE Transactions on Geoscience and Remote Sensing*, *42*(12), 2747–2760. https://doi.org/10.1109/TGRS.2004.836388

Chen, J., & Zhu, W. (2022). Comparing Landsat-8 and Sentinel-2 top of atmosphere and surface reflectance in high latitude regions: case study in Alaska. *Geocarto International*, *37*(20), 6052–6071. https://doi.org/10.1080/10106049.2021.1924295

Concha, J., Mannino, A., Franz, B., Bailey, S., & Kim, W. (2019). Vicarious calibration of GOCI for the SeaDAS ocean color retrieval. *International Journal of Remote Sensing*, *40*(10), 3984–4001. https://doi.org/10.1080/01431161.2018.1557793

Ellis, D. C. S. & J. (2014). *Stats Tutorial - Instrumental Analysis and Calibration*. Department of Chemistry, University of Toronto.

ESA. (1956). Sentinel-2 User Handbook. In *ESA* (Vol. 48, Issue 9). https://doi.org/10.1021/ie51400a018

Falls, S. (2010). OPERATIONAL CALIBRATION AND VALIDATION OF LANDSAT DATA CONTINUITY MISSION (LDCM) SENSORS USING THE IMAGE ASSESSMENT SYSTEM (IAS) Esad Micijevic and Ron Morfitt SGT Inc .,* Contractor to the U . S . Geological Survey (USGS) Earth Resources Observatio. *Work*, *Ldcm*, 2291–2294.

Helder, D. L., Malla, R., Mettler, C. J., Markham, B. L., & Micijevic, E. (2012). Landsat 4 thematic mapper calibration update. *IEEE Transactions on Geoscience and Remote Sensing*, *50*(6), 2400–2408. https://doi.org/10.1109/TGRS.2011.2171350

Inggit Lolita Sari, Tatik Kartika, K. (2011). Kajian Forest Base Probability Menggunakan Citra Landsat untuk Mendukung Indonesia's National Carbon Accounting System (INCAS) Wilayah Sumatera. *Seminar Nasional Pemanfaatan Data Penginderaan Jauh Untuk Mendukung Pembangunan Nasional*.

Junaidi. (2010). Titik Persentase Distribusi t. In *Http://Junaidichaniago.Wordpress.Com*. http://ledhyane.lecture.ub.ac.id/files/2013/04/tabel-t.pdf

Liu, Y., Ma, L., Wang, N., & Qian, Y. (2017). Vicarious radiometric calibration/validation of Landsat-8 operational land imager using a ground reflected radiance-based approach with Baotou site in China. *Journal of Applied Remote Sensing*, *11*(04), 1. https://doi.org/10.1117/1.jrs.11.044004

Lu, J., He, T., Liang, S., & Zhang, Y. (2022). An Automatic Radiometric Cross-Calibration Method for Wide-Angle Medium-Resolution Multispectral Satellite Sensor Using Landsat Data. *IEEE Transactions on Geoscience and Remote Sensing*, *60*, 1–11. https://doi.org/10.1109/TGRS.2021.3067672

Malvern Panalytical. (2022). *ASD FieldSpec 4 Brochure*. https://www.malvernpanalytical.com/en/products/product-range/asd-range/fieldspec-range/fieldspec-4-standard-res-spectroradiometer

Markham, B. L., Knight, E. J., Canova, B., Donley, E., Kvaran, G., Lee, K., Barsi, J. A., Pedelty, J. A., Dabney, P. W., & Irons, J. R. (2012). The Landsat Data Continuity Mission Operational Land Imager (OLI) sensor. *International Geoscience and Remote Sensing Symposium (IGARSS)*, 6995–6998. https://doi.org/10.1109/IGARSS.2012.6351961

Martimort, P., Fernandez, V., Kirschner, V., Isola, C., & Meygret, A. (2012). *SENTINEL-2 MULTISPECTRAL IMAGER (MSI) AND CALIBRATION / VALIDATION (1) European Space Agency , ESTEC , Noordwijk , Netherlands (2) Centre National d ' Etudes Spatiales , Toulouse , France*. *1*, 6999–7002.

Ong, C., Malthus, T., Lau, I. C., Thankappan, M., & Byrne, G. (2018). The development of a standardised validation approach for surface reflectance data. *International Geoscience and Remote Sensing Symposium (IGARSS)*, *2018-July*, 6456–6459. https://doi.org/10.1109/IGARSS.2018.8518624

Pal, M. K., & Porwal, A. (2015). Spectral noise reduction and smoothing using local cubic least square regression from hyperion reflectance data. *2nd International Conference on Signal Processing and Integrated Networks, SPIN 2015*, 752–755. https://doi.org/10.1109/SPIN.2015.7095401

Raut, B., Kaewmanee, M., Angal, A., Xiong, X., & Helder, D. (2019). Empirical absolute calibration model for multiple pseudo-invariant calibration sites. *Remote Sensing*, *11*(9). https://doi.org/10.3390/rs11091105

Salaswati, S., Anggari, E. A., Fakhlevi, M. R., & Pamadi, B. S. (2021). Potential Area for Radiometric Calibration of Satellite Cameras in Indonesia. *2021 IEEE International Conference on Aerospace Electronics and Remote Sensing Technology (ICARES)*, 1–7. https://doi.org/10.1109/ICARES53960.2021.9665190

Sari, I. L., Weston, C. J., Newnham, G. J., & Volkova, L. (2022). Using Bayesian multitemporal classification to monitor tropical forest cover changes in Kalimantan, Indonesia. *International Journal of Digital Earth*, *15*(1), 2061–2077. https://doi.org/10.1080/17538947.2022.2146219

Setiyoko, A., Hendayani, Sulyantara, H., Maryanto, A., Suhermanto, Dianovita, Musyarofah, Luthfi, H. A., Vallianto, B., Kiki Winda Veronica, & Adestia, R. (2023). Spectral Reflectance Initial Analysis of Bromo Sand for Landsat 9 Calibration Validation. *IEICE Technical Report*, 17–22. https://www.ieice.org/publications/ken/summary.php?contribution_id=127843&society_cd=ISS&ken_id=IE&year=2023&presen_date=2023-12-07&schedule_id=7955&lang=en&expandable=3

Song, Q., Ma, C., Liu, J., Wang, X., Huang, Y., Lin, G., & Li, Z. (2022). Time Series Analysis-Based Long-Term Onboard Radiometric Calibration Coefficient Correction and Validation for the HY-1C Satellite Calibration Spectrometer. *Remote Sensing*, *14*(19). https://doi.org/10.3390/rs14194811

Tang, H., Xie, J., Tang, X., & Li, Q. (2019). Radiometric Cross-calibration of ZY3 Satellite with GF1 PMS/WFV and Landsat-8 OLI. *International Geoscience and Remote Sensing Symposium (IGARSS)*, 9006–9009. https://doi.org/10.1109/IGARSS.2019.8898912

Teixeira Pinto, C., Haque, M. O., Micijevic, E., & Helder, D. L. (2019). Landsats 1-5 multispectral scanner system sensors radiometric calibration update. *IEEE Transactions on Geoscience and Remote Sensing*, *57*(10), 7378–7394. https://doi.org/10.1109/TGRS.2019.2913106

Trevisiol, F., Mandanici, E., Pagliarani, A., & Bitelli, G. (2024). Evaluation of Landsat-9 interoperability with Sentinel-2 and Landsat-8 over Europe and local comparison with field surveys. *ISPRS Journal of Photogrammetry and Remote Sensing*, *210*(February), 55–68. https://doi.org/10.1016/j.isprsjprs.2024.02.021

USGS. (2022). Landsat 9 Data Users Handbook Version 1.0. In *Nasa* (Issue February). https://d9-wret.s3.us-west-2.amazonaws.com/assets/palladium/production/s3fs-public/media/files/LSDS-2082_L9-Data-Users-Handbook_v1.pdf

Zhang, C., Jia, S., & Wu, Y. (2021). ON SIMULTANEOUS CALIBRATION OF TWO-SAMPLE t-TESTS FOR HIGH-DIMENSION LOW-SAMPLE-SIZE DATA. *Statistica Sinica*, *31*(3), 1189–1214. https://www.jstor.org/stable/27034814

Zhu, S., Li, Z., Qie, L., Xu, H., Ge, B., Xie, Y., Qiao, R., Xie, Y., Hong, J., Meng, B., Tu, B., & Chen, F. (2022). In-Flight Relative Radiometric Calibration of a Wide Field of View Directional Polarimetric Camera Based on the Rayleigh Scattering over Ocean. *Remote Sensing*, *14*(5), 1–19. https://doi.org/10.3390/rs14051211